Journal of Power Sources 196 (2011) 7707–7714

Contents lists available at ScienceDirect

Journal of Power Sources

journal homepage: www.elsevier.com/locate/jpowsour

A comparative study of polyacrylic acid and poly(vinylidene difluoride) binders for spherical natural graphite/$LiFePO_4$ electrodes and cells

Jin Chong[a,b], Shidi Xun[a,*], Honghe Zheng[a], Xiangyun Song[a], Gao Liu[a], Paul Ridgway[a], Ji Qiang Wang[b], Vincent S. Battaglia[a]

[a] Lawrence Berkeley National Laboratory, Berkeley, CA 94720, USA
[b] Tianjin Institute of Power Sources, Tianjin, 300381, China

ARTICLE INFO

Article history:
Received 15 March 2011
Received in revised form 18 April 2011
Accepted 19 April 2011
Available online 23 April 2011

Keywords:
Spherical natural graphite
LiFePO4
Aqueous based binder
Lithium-ion batteries

ABSTRACT

Anodes containing spherical natural graphite (SNG12) and cathodes containing $LiFePO_4$, both from HydroQuebec, were prepared with aqueous-based polyacrylic acid (PAAH), its neutralized derivatives polyacrylic acid (PAAX) (X = Li, Na, and K), and with conventional poly(vinylidene difluoride) (PVDF) binders. A comparison of electrode performance was made between these three binder systems. The electrodes were optimized by adding elastic styrene butadiene rubber (SBR) and conductive vapor grown carbon fiber (VGCF) in the place of some of the PAAX. Initially, SNG12 and $LiFePO_4$ electrodes were characterized in half cells with Li as the counter electrode. The electrochemistry results show that the use of PAAX binders can significantly improve the initial coulombic efficiency, reversible capacity, and cyclability of SNG12 anodes and $LiFePO_4$ cathodes as compared to that of electrodes based on a PVDF binder. By using an optimized composition for the anode and cathode, SNG12/$LiFePO_4$ full cells with PAALi binder cycled 847 times with 70% capacity retention, which was a significant improvement over the electrodes with PVDF (223 cycles). This study demonstrates the possibility of manufacturing Li-ion batteries that cycle longer and use water in the processing, instead of hazardous organic solvents like NMP, thereby improving performance, reducing cost, and protecting the environment.

1. Introduction

For composite electrodes of lithium-ion batteries, binders provide two important functions, holding together the active materials and additives into a cohesive, conductive laminate, and providing the adhesion between the laminate and the current collector. Because the surface chemistry and morphology of electrode materials vary, optimization of the binder system for different electrode materials is part of the routine in the development of high performance batteries. As of today, poly(vinylidene difluoride) (PVDF) binder is the most widely used binder for Li-ion cells. This is due to its good electrochemical stability and binding capability, and ability to absorb electrolyte for facile transport of Li to the active material surface [1–6]. However, the cost of PVDF-based electrodes is still a concern in the battery industry as PVDF is processible into electrodes only by solubilizing it in an organic solvent to form a castable, viscous slurry. The environmental impacts of such a process range from questionable to toxic [7]. Thus, lots of effort has been put toward the pursuit of an environment-friendly, cost-effective binder for lithium-ion batteries, such as carboxymethyl cellulose (CMC) [7–18] and polyacrylic acid (PAAH) [19,20]. The chemical structures of these two polymers are shown in Fig. 1 along with that of PVDF for comparison.

As an alternative binder to PVDF, CMC (mainly as its sodium neutralized derivative) has been extensively investigated in Si [13–17] and natural graphite anodes [18], and in $LiFePO_4$ cathodes [7–12]. CMC's effectiveness with selected electrode materials may result from the formation of ester-like chemical bonding between the CMC molecules and the OH groups native to the SiO_2 layer found on the Si surface [14,15], or its extended conformation in solution that facilitates an interlinked network of conductive additive and Si particles during the composite electrode elaboration [21], or the improved compatibility with the electrode materials [7]. Similar functionality is found for aqueous-based PAAH binder; however, compared to CMC, PAAH has not received nearly as much attention. PAAH as binder for Sn alloy and graphite anodes has previously been reported [19,20] and an attempt was made to employ PAAH as a dispersant for $LiFePO_4$ electrodes [12]. However, to the best of our knowledge, PAAH as a binder for Li-ion batteries nor its salt derivatives has been fully explored, especially with regard to addition of a second polymer, and we have found no reports on cells where both electrodes were cast from aqueous solutions.

In this study, aqueous-based PAAH binder and its derivatives [PAALi, PAANa, and PAAK with the addition of styrene butadiene

* Corresponding author. Tel.: +1 510 4866586; fax: +1 510 4864260.
E-mail address: sxun@lbl.gov (S. Xun).

0378-7753/$ – see front matter © 2011 Elsevier B.V. All rights reserved.
doi:10.1016/j.jpowsour.2011.04.043

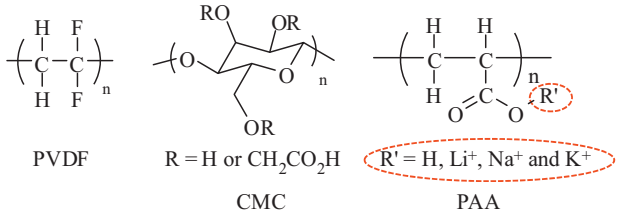

Fig. 1. Chemical structures of binders.

rubber (SBR)] for both electrodes of the natural graphite/$LiFePO_4$ battery system were investigated. This electrochemical couple was selected for investigation because it is potentially of low cost and of relatively high stability [2]. A half-cell evaluation of PAAX (X = H, Li, Na, or K) for SNG12 anodes was performed and compared to an anode with PVDF. $LiFePO_4$ cathodes based on PAALi and PVDF were also investigated in half cells. Finally, the suitability of a battery of PAALi in both electrodes was compared to PVDF in SNG12/$LiFePO_4$ full cells.

2. Experimental

2.1. Materials

The spherical natural graphite (SNG12) used in this study is a product of Hydro-Quebec. It was fabricated through a purification and processing step that results in the folding of the graphite fragments into small spheres to solve the problem of the intolerance of the electrolyte with the edge planes of the highly orientated graphitic layers [2,11]. The average particle size of SNG12 is in the range of 10 μm to 15 μm, with the largest being no more than 20 μm. The $LiFePO_4$ powders were also provided by Hydro-Québec. The average particle size of the $LiFePO_4$ was about 0.1 μm with the largest being no more than 0.5 μm. Battery grade acetylene black (AB) with an average particle size of 40 nm was acquired from Denka Singapore Private, Limited. Polyacrylic acid powder with an average molecular weight of 450,000 was purchased from Sigma–Aldrich. PAALi, PAANa, and PAAK binders were made from polyacrylic acid by stoichiometrically neutralizing it with lithium hydroxide, sodium hydroxide, and potassium hydroxide, respectively. The lithium hydroxide (99.9%), sodium hydroxide (98.5%), and potassium hydroxide (99.99%) were purchased from Sigma–Aldrich. PVDF (no. 1100) binder was supplied by Kureha, Japan. Anhydrous 1-methylpyrrolidinone (NMP) was purchased from Sigma–Aldrich. Vapor-grown carbon fiber (VGCF) and acetylene black (AB) were supplied by Showa Denko Carbon, Inc. Aqueous solutions of 40% SBR were obtained from Asahi Chemicals, Japan. An electrolyte of 1 M $LiPF_6$ in EC: DEC, 1:2 by mass, was purchased from Novolyte Technologies, Inc.

2.2. Electrode preparation

Measured amounts of active material, AB or VGCF, and binder were added to a beaker with suitable amounts of solvent (NMP for PVDF, deionized water for PAAH, PAALi, PAANa, and PAAK). The components were combined using a Polytron PT 10-35 homogenizer at 3000 rpm for 10 min until uniform. The anode slurries were coated onto copper foil current collectors and the cathode slurries onto aluminum foil current collectors with the use of a doctor-blade. The laminate loading was controlled by the height of the doctor-blade. After the laminates were dried at 40 °C in air for 30 min, they were calendered to 30% porosity. The calendered laminates were then either punched into 1.429 cm diameter anodes or 1.270 cm diameter cathodes. The punched electrodes were dried under vacuum at 140 °C for 16 h in an antechamber attached to an argon atmosphere glovebox and then transferred into the glovebox.

2.3. Electrode characterization

The morphology of powders and electrodes were imaged with a JEOL JSM-7500F field emission scanning electron microscope (SEM). The electrode surface chemistry was mapped with an energy dispersive X-ray (EDX) analyzer from Thermo Scientific Analysis. The electronic conductivities of the electrode films were measured using the four-point probe DC method, as described in ref. [22]. The films to be tested were peeled off the current collector, applied to a glass substrate, and vacuum dried at 140 °C for 16 h. The DC conductivity measurement was then performed using a custom-built, equidistant, four-point-probe apparatus with a Solartron 1286 Electrochemical Interface and CorrWare software. The probes were spring loaded to ensure intimate contact with the film. A direct current was applied between the two outer probes; the voltage was measured between the two inner probes. The conductivity of each film was measured three times at different locations on the film. The film thickness was measured using a Mitutoyo micrometer. The thickness was measured 3 times and the average used in the estimation of the conductivity.

2.4. Electrochemical measurements

The charge–discharge tests were performed in CR2325 coin cell hardware. Half cells consisted of the electrode to be studied, Li metal as the counter electrode, and Celgard 2400 separator. Full cells were made with SNG12 anodes, $LiFePO_4$ cathodes, and the same separator. An electrolyte of 1 M $LiPF_6$ in EC:DEC, 1:2, was added to all of the cells. Anode half-cells were tested between 1.0 V and 0.005 V at a discharge (lithiation) rate of 0.05 C. Cathode half-cells were tested between 2.2 V and 3.9 V with a charge rate of 0.1 C. After 10 cycles, a *C*-rate test was performed which consisted of currents of 0.1 C, 0.2 C, 0.5 C, 1 C, 2 C, 5 C, 10 C, and 20 C in consecutive cycles. Full cells were tested between 2.2 V and 3.9 V with a charge/discharge rate of 1 C. All of the cell tests were performed with a Maccor 4000 battery tester in an environmental chamber from Testequity (model TEC1) set at 30 (±2) °C.

3. Results and discussion

3.1. Electrode morphology

The morphology of the electrodes in this study was characterized by using SEM and EDX mapping techniques. Fig. 2 shows the SEM images of SNG12 and $LiFePO_4$ electrodes with different binders (PVDF and PAANa binders for the SNG12 electrodes, PVDF and PAALi binders for the $LiFePO_4$ electrodes). The SEM showed that the SNG12 particles were composed of many small graphite domains and that the average diameter of the particles was about 12 μm. Since PVDF contains fluorine and PAANa contains sodium, the mapping of fluorine and sodium with EDX made it easy to visualize the distribution of PVDF and PAANa binders in the electrodes. The inset of the figures shows that both PVDF and PAANa binders completely coat the SNG12 particles. In contrast to PVDF, polymer bridges were observed between particles with the PAANa binder (marked with a dashed-circle in Fig. 2b), which has previously been seen for CMC on graphite [18]. Similar phenomenon was observed when the PAALi binder was mixed with SNG12 (SEM not shown). The PAAK binder, however, did not appear to coat the SNG12 particles and instead deposited in the interspaces between the particles. For the two $LiFePO_4$ cathodes (Fig. 2c and d), a homogenous distribution of active material and carbon additive was achieved; the main difference between these two electrodes was that the one

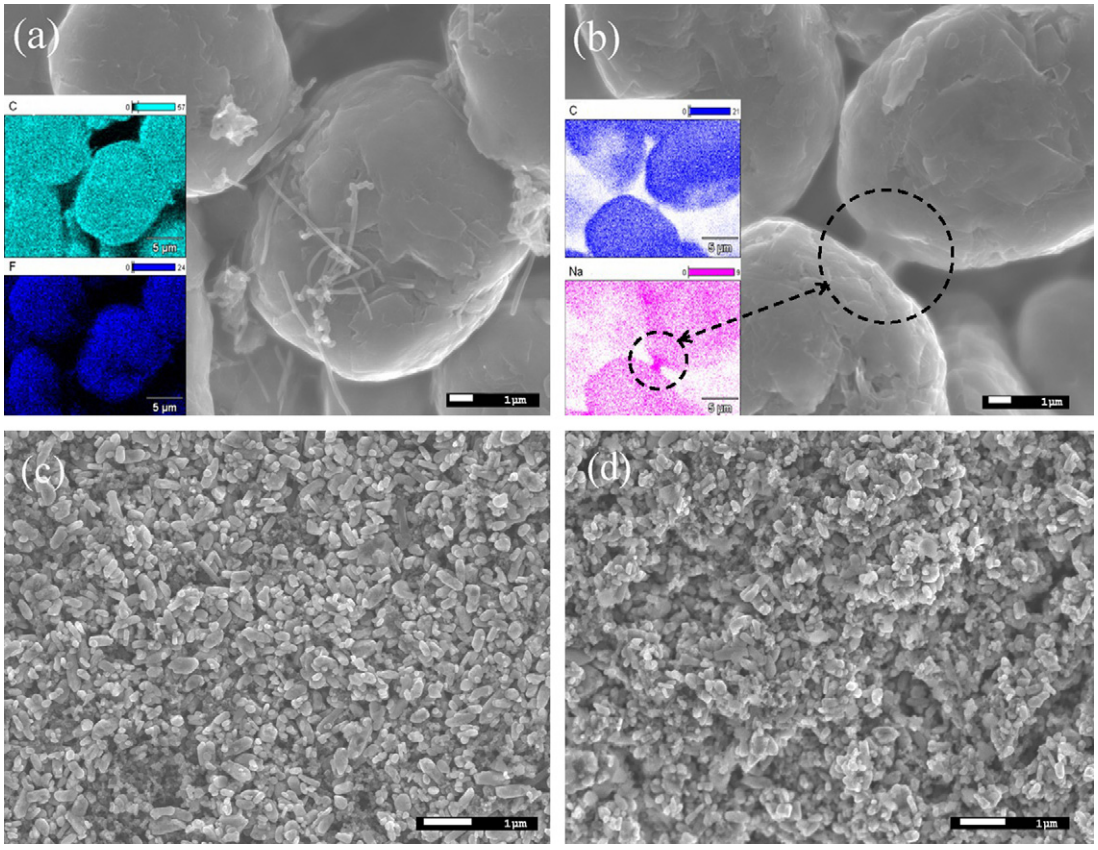

Fig. 2. SEM image and EDX mapping of SNG12 with (a) SNG12 (86%)/PVDF (10%) /AB (2%)/VGCF (2%), (b) SNG12 (90%)/PAANa (10%) (c) LiFePO4 (82%)/ PVDF (10%)/AB (8%) (d) LiFePO4 (82%)/PAALi (9%)/AB (8%)/SBR (1%).

made with PAALi had a higher void fraction after casting. This was probably due to the foaming that occurs during the mixing of aqueous-based binder systems and led to a much more porous structure upon casting and after drying.

It is known that CMC aqueous binder is extremely stiff and brittle [20]; after vacuum drying, large cracks are plainly visible and the laminates easily slide off of the current collector. As reported [17], addition of the elastomeric additive SBR to CMC results in electrodes that are less brittle and, compared to PVDF, show a smaller Young's modulus, a larger maximum elongation, a stronger adhesion strength to the current collectors, but less absorption of the organic carbonate electrolyte [13]. PAA(H, Li, and Na) binders are similar to CMC in these regards. Heretofore, SBR was added to the PAA(H, Li, Na or K) binder systems as a means of improving the physical characteristics of the electrodes.

3.2. SNG12 anode electrochemical performance

To evaluate the electrodes, half cells were assembled and tested. Fig. 3 shows the first ten cycles of SNG12 with different binders, cycled at a rate of 0.05 C. The electrode composition with the PVDF binder was SNG12 (86%)/PVDF (10%)/AB (2%)/VGCF (2%) and with the PAAX binders was SNG12 (90%)/PAA(H, Li, Na, or K) (10%). The reversible specific capacity achieved was 340 mAh g^{-1} if PAALi, PAANa, or PAAK binder was used. Even with PAAH binder, a respectable specific capacity of 315 mAh g^{-1} was obtained, which was slightly lower than that found with the PVDF binder (320 mAh g^{-1}). The first-cycle coulombic-efficiency of the cells with PAAH, PAAK, and PVDF was lower than 90%, but as high as 92.6% and 92.8% with PAALi and PAANa, respectively. For cyclability, capacity fade wasn't observed during the first 10 cycles. Thus, compared to PVDF, PAA(Li and Na) binders showed higher initial efficiency and reversible capacity, which may be a result of the coatability of these binders.

In addition to the electrode's mechanical properties, "good" SEI formation is a key parameter governing cell performance [23]. For PVDF, 70% of the SEI is formed in the first cycle [24], and requires several subsequent cycles to form a stable interface [20]. A more effective and stable SEI layer appeared to form in fewer cycles with the PAAX binders [20]. For the PAAX, the Li, Na, or K dissociates, leaving negative charges on the polymer chains that suppress the aggregation of the polymer through electrostatic repulsion [19]. For the PAAH, strong hydrogen–hydrogen bonds may form in the aqueous solutions among polymer strands that do not fully dissociate

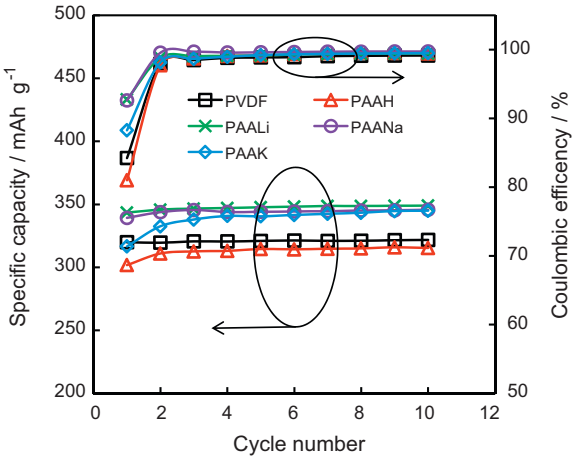

Fig. 3. The cycle performance of SNG12 anode with different binders.

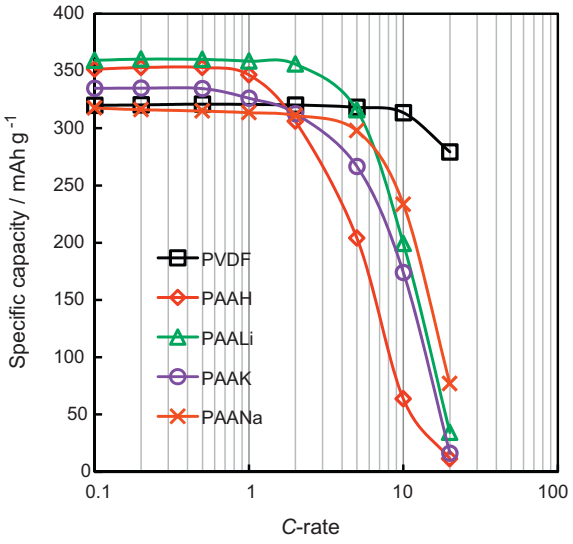

Fig. 4. The *C*-rate performance of SNG12 anode with different binders.

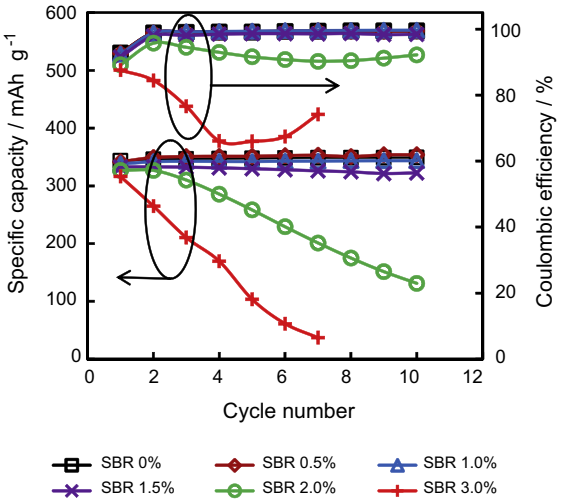

Fig. 6. The cycle performance of SNG12 anode with PAALi binder doped by different amounts of SBR.

with the proton, leading to the aggregation of some of the polymer. This can lead to loss of useable polymer and zones of inactivity. With less polymer aggregation, a more homogenous coating may be obtained. Among the PAAX systems, PAAK is worse than PAANa and PAALi. The PAAK with SNG12 appeared to clump and not uniformly coat the graphite as well as that found using PAALi and PAANa, and resulted in a slightly lower initial coulombic efficiency and reversible capacity. This appears to be more of a processing issue with PAAK requiring additional efforts in determining a more suitable mixing procedure.

As power is a critical factor for vehicular applications, the *C*-rate performance of the electrodes with different binders was tested, as shown in Fig. 4. The loading was controlled in the range from 1.04 to 1.26 mAh cm^{-2}. All anodes were discharged (lithiated) at 0.1 C and charged from 0.1 C to 20 C. Among all of the binder systems, PVDF showed the best capacity retention at higher rates (83% at 20 C), which was attributed to the higher absorption of the organic electrolytes with this polymer, as mentioned earlier. PVDF swells with the intake of electrolyte and makes for a less encumbered pathway for Li-ions to access the electrode, whereas the PAAX binders are not as absorbant of the electrolyte, producing a film that tends to impede Li-ion transport to the active material surface.

Since the cells with PAALi binder showed the highest capacity and lowest first cycle loss, this chemistry was selected to be doped with different amounts of SBR to determine if the addition of a more flexible binder could improve on the cracking. The active material's fraction was held constant at 90%, the SBR was adjusted from 0 to 3%, and, correspondingly, the PAALi was adjusted from 10 to 7%. With regard to physical properties, the electrodes with 1% or more SBR showed no visible cracks after drying. Fig. 5 provides a comparison of an electrode with and without SBR from an SEM at low magnification. Cracks are clearly visible in the electrode without SBR.

Fig. 6 shows the charge capacity and coulombic efficiency of the first 10 cycles of SNG12 anode with PAALi binder substituted with different amounts of SBR. The cells were cycled at 0.05 C. The initial coulombic efficiency was unaffected by the increase of the SBR content up to 1.5%, beyond which the first cycle efficiency dropped. At 3.0% SBR, the first cycle efficiency was measured at 87.6% as compared to 92.8% for 0% SBR. Almost the same reversible capacity and columbic efficiency was obtained with SBR from 0% to 1.0% and no capacity fade was measured for the first 10 cycles. However, when the SBR content exceeded 1.0%, the reduction in cycling capability was measurable. Too much substitution of SBR for PAALi may interfere with the connecting bridges formed by the PAALi between the active particles, which then may lead to particle isolation with cycling.

To verify this prognosis, the electronic conductivity of the electrodes with different amounts of SBR was measured with a 4-point-probe. Fig. 7 shows the conductivity of SNG12 anodes with PAALi binder doped with different amounts of SBR, where, again, the content of the SNG12 was held at 90%. Also shown is that the electrode with PAANa binder had almost the same conductivity (0.61 S cm^{-1}) as that of PAALi but that the electrode with PAAK was half as much at 0.32 S cm^{-1}. This may explain why the cells based on PAAK in Figs. 3 and 4 did not perform as well as those based on PAALi and PAANa.

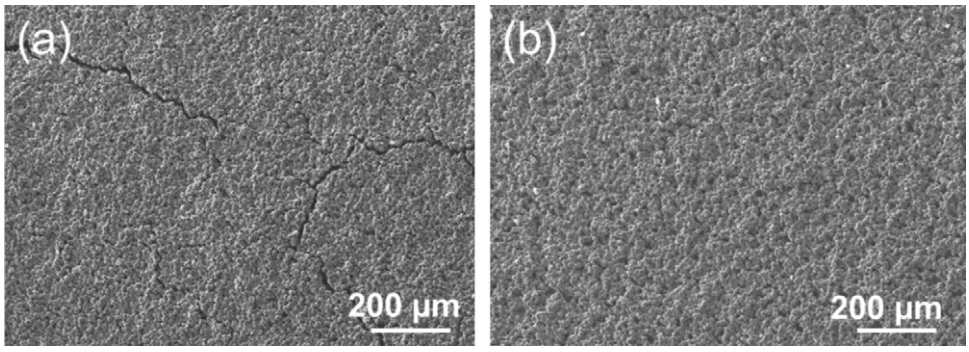

Fig. 5. Anodes of SNG12 with PAALi binder. (a) SNG12 (90%)/PAALi (10%), (b) SNG12 (90%)/ PAALi (9%)/ SBR (1%).

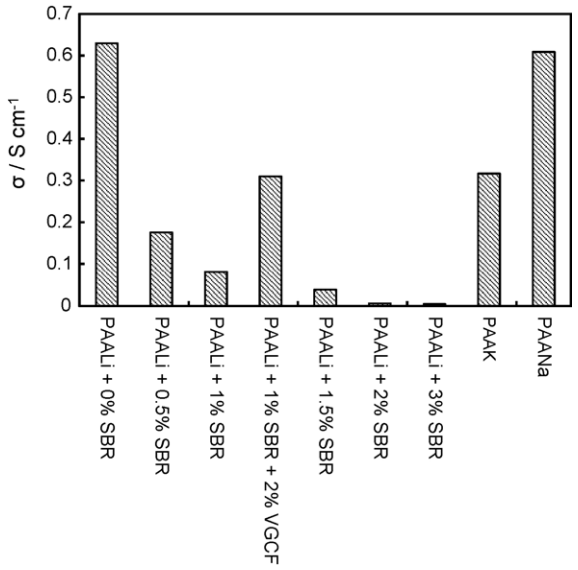

Fig. 7. The conductivity of SNG12 anode with different binders.

This data confirmed that the conductivity decreased monotonically with the addition of SBR. With the electrolyte having a conductivity on the order of 0.01 S cm^{-1}, to minimize the impact on the ohmic resistance, the electronic conductivity should be kept at least an order of magnitude greater than this value. Compared to the electrode without SBR, the conductivity of an electrode with 1.0% SBR decreased from 0.63 S cm^{-1} to 0.08 S cm^{-1}. Addition of even more SBR pushed the conductivity below this prescribed cut-off. For this reason, 1.0% SBR was selected as the right balance between good physical properties (no cracks) and good rate performance. Thus, an electrode of 90% active material, 9% PAALi, and 1% SBR was selected for further evaluation.

In order to improve the conductivity of electrodes containing 1% SBR, VGCF (2%) was substituted for active material. In so doing, the conductivity was increased nearly a factor of 4–0.31 S cm^{-1}. Fig. 8a shows the SEM image of the anode with PAALi binder (9%) doped with SBR (1.0%) and VGCF (2%); the anode particles appear to be interconnected by the long VGCF. The electrode is described schematically in Fig. 8b and c. Without VGCF, even if the SNG12 particles were initially held together by the binder, some particles may still become electronically isolated with cycling. The addition of the VGCF, (Fig. 8c), helped to both establish and maintain electronic connections between particles. Another possible benefit of a fiberous additive would be its ability to strengthen the electrodes mechanical properties in the same way that rebar strengthens concrete.

As further evidence that the electronic conductivity of these electrodes played an important role in their rate capability, the

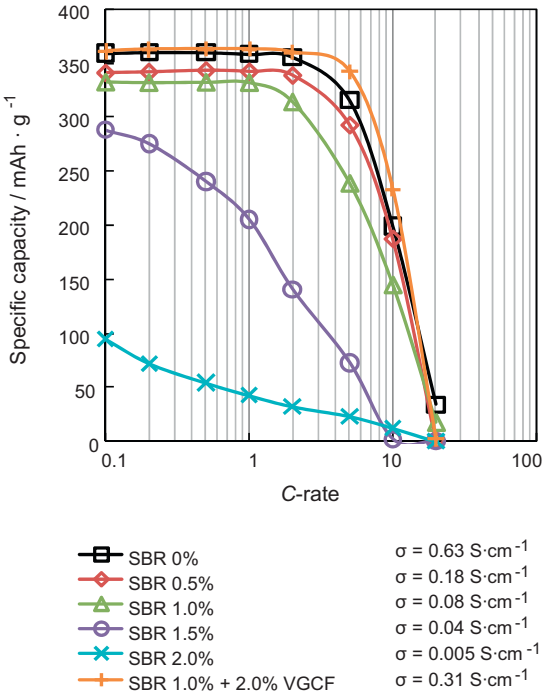

Fig. 9. The *C*-rate performance of SNG12 anode with PAALi binder doped by different amounts of SBR or VGCF.

C-rate performance of the SNG12 anode with PAALi binder doped with different amounts of SBR are shown in Fig. 9. The electrode loadings for these tests were held nearly constant in the range of 1.04–1.26 mAh cm^{-2}. The electrode's *C*-rate capability declined significantly when the electrode conductivity dropped below 0.08 S cm^{-1} (1% SBR). The addition of the VGCF bolstered the electrode's capability to its highest level. When 2.0% VGCF was substituted into the electrode with 1.0% SBR, the capacity at 5 C rebounded from 71.7% to 94.7%. In summary, the addition of SBR leads to electrodes without cracks and better adhesion to the current collector but poorer electronic conductivity that can be recovered by the addition of VCGF. Based on this cycling and rate performance testing, the chosen composition for SNG12 anodes for follow-on cycleability tests was SNG12 (88%)/PAALi (9%)/SBR (1%)/VGCF (2%).

3.3. $LiFePO_4$ cathode electrochemical performance

Cathodes of $LiFePO_4$ with PAALi binder were also investigated. As discussed in the development of the anodes, the PAAX binder alone lead to brittle electrodes; they fractured, which resulted in a few, small, isolated fragments of active material. When elastic SBR

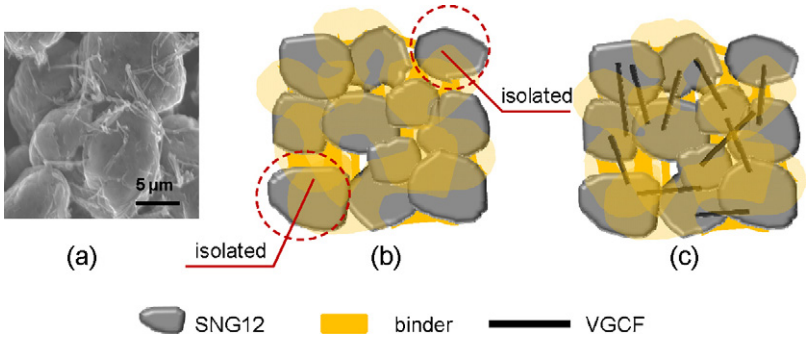

Fig. 8. SEM image of electrode with PAALi binder doped by 1.0% SBR and 2% VGCF (a) and cartoon graph for electrode without VGCF (b) with VGCF (c).

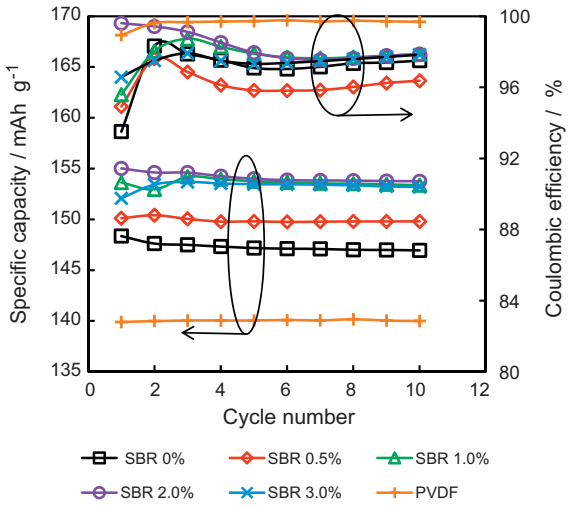

Fig. 10. The cycle performance of LiFePO4 cathode with PVDF binder and PAALi binder doped by different amounts of SBR.

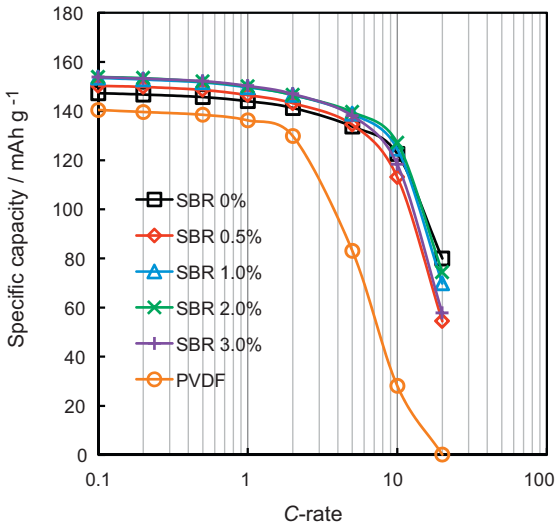

Fig. 11. The *C*-rate performance of LiFePO4 cathode with PVDF binder and PAALi binder doped by different amounts of SBR.

was introduced, electrodes with good morphologies were obtained. Thus, it was anticipated that the cathodes would require some level of SBR. Since PAAH contains hydrogen groups that could dissociate to some degree in electrolyte and in turn lead to etching of the cathode active material, PAAH was not considered for the cathode as binder. In addition, as no advantages were seen for the other PAAX binders over PAALi in the anode, PAALi was selected for optimization for the cathode. The composition was always $LiFePO_4$ (82%)/AB (8%)/(PAALi + SBR) (10%). Please note the addition of carbon black to all electrodes. This was done because $LiFePO_4$ is known to be a poor electronic conductor, unlike graphite. In general, the levels of inactive components were held at reasonably low levels in order to maintain the energy density. Fig. 10 shows the first 10 cycles of $LiFePO_4$ cathodes with PAALi binder substituted for different amounts of SBR and with PVDF binder as reference. With PAALi binder, the reversible capacity increased from 147 mAh g^{-1} to 155 mAh g^{-1} when SBR levels increased from 0% to 2.0%. The slight increase was likely a result of reduced electrode fracturing with the addition of SBR. The $LiFePO_4$ electrode with 2.0% SBR showed an initial columbic efficiency of 89.6%. When the SBR amount reached 3.0%, the reversible capacity and columbic efficiency slightly decreased. Similar to the SNG12 electrodes, the decrease in reversible capacity and columbic efficiency was probably due to the insulating effects of excessive amounts of SBR. However, the $LiFePO_4$ electrodes did not lose as much capacity as the SNG12 electrodes did with the addition of SBR, which suggests that the conductive additive content could be lowered in some future efforts. The cells were tested at 0.1 C. The reversible capacity obtained for the PVDF-based electrode was 140 mAh g^{-1}, there is no explanation for this discrepancy. The cycling performance against Li-metal is stable.

The rate performance of $LiFePO_4$ cathodes with PAALi and SBR were tested for their rate capability, as shown in Fig. 11. The loading was controlled in the range of 0.95–1.10 mAh cm^{-2}. The cells were charged at 0.1 C and discharged from 0.1 C to 20 C. There was no obvious variation of rate capability observed for the cathodes with different SBR doping, which may be due to the effective conductive pathways provided by AB in the electrodes. Reversible capacities of between 77% (3% SBR) and 83% (0% SBR) were retained at 10 C. For comparison, an electrode with PVDF binder ($LiFePO_4$ 82%, PVDF 10% and AB 8%) was prepared and tested. At a 10 C discharge rate, only 20% of the reversible capacity was retained.

Overall, electrodes doped with 1% SBR and 2% SBR possessed almost the same rate capability and, for the initial 10 cycles, the cell based on 2% SBR was slightly better than that based on 1%. However, considering that SBR is electronically insulting, minimizing its use was preferred. Thus, the electrode with PAALi binder doped by 1.0% SBR was selected as the cathode composition for full cell evaluation.

3.4. SNG12/$LiFePO_4$ full cell cycling

After the optimization of the anode and cathode in half cells, full cells were assembled to further evaluate PAALi binder for longer-term cyclability and to compare it with cells made with PVDF binder. All of the full cells were designed to be cathode limited on charge, where the anode capacity was approximately 110% of

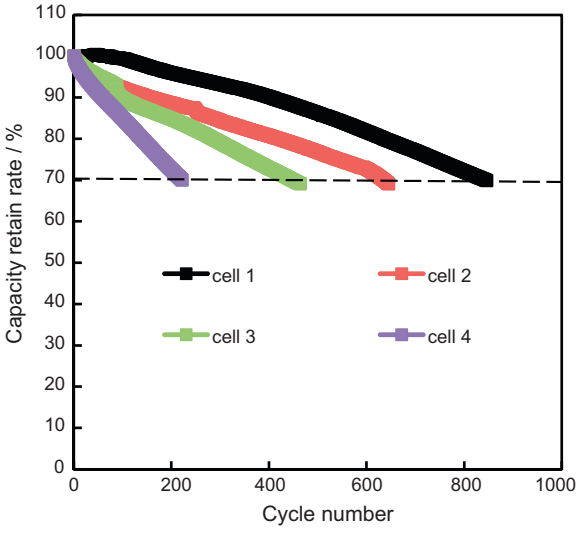

Cell1: anode: 9% PAALi/1% SBR/2% VGCF/88% SNG12
cathode: 9% PAALi/1% SBR/8% AB/82% $LiFePO_4$
Cell 2: anode: 9% PAALi/1% SBR/90% SNG12
cathode: 10% PVDF/8% AB/82% $LiFePO_4$
Cell 3: anode: 10% PAALi/90% SNG12
cathode: 10% PVDF/ 8% AB/82% $LiFePO_4$
Cell 4: anode: 10% PVDF/2% AB/2% VGCF/86% SNG12
cathode: 10% PVDF/8% AB/82% $LiFePO_4$

Fig. 12. Full cells cycling performance of the SNG12/LiFePO4 couple with different binders.

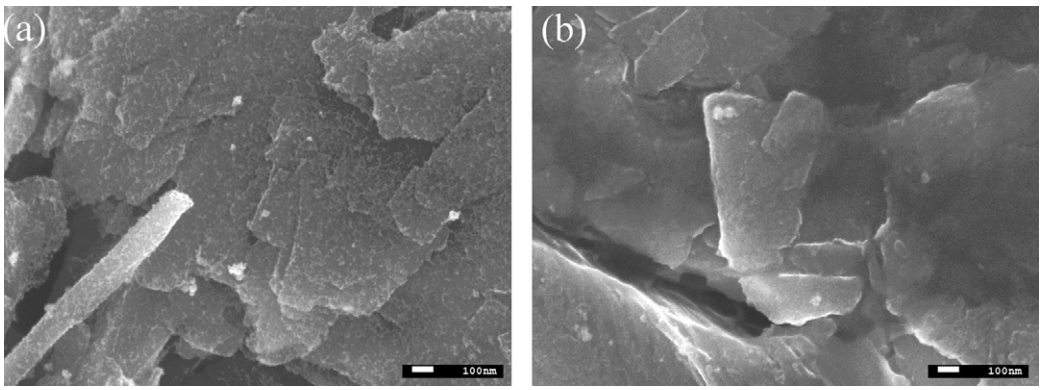

Fig. 13. The SEM images of cycled SNG12 anodes in full cells (a) cell 4 (b) cell 1.

cathode capacity. For cycle life testing, end-of-life was defined as 30% loss of initial capacity. Fig. 12 shows cycling performance of the SNG12/$LiFePO_4$ with different binders. The first cell contained the inactive materials PAALi, SBR, and VCGF in the anode, and PAALi, SBR, and AB in the cathode. The cathode for the other three cells tested contained PVDF and AB. The anode for cell 2 did not have VCGF and the anode for cell 3 did not contain either SBR or VCGF. Finally, the 4th cell consisted of PVDF-based anode.

The full cell utilizing PVDF binder in both electrodes (cell 4) cycled the fewest number of cycles (223) before reaching end-of-life. The full cell using an optimized amount of PAALi in both electrodes (cell 1) cycled the most times at 847. This cell had the following formulation: SNG12 anode with 9% PAALi binder, 1.0% SBR, and 2.0% VGCF; and $LiFePO_4$ cathode with 8% AB, 9% PAALi binder, and 1.0% SBR.

As indicated in the half cell experiments, the SNG12 anode performance was influenced much more by the binder and conductive additive content than the cathode. The cyclablity of cells 2, 3, and 4 appeared strongly dependent on the anode performance as well, as each consisted of a cathode of the same composition. When the PVDF was replaced with PAALi in the anode (cell 3), the cyclability increased from 223 to 447 cycles. When some of the PAALi was replaced with SBR in the anode, the cyclability increased again to 635 cycles (cell 2).

It is known that an effective SEI layer is critical to a high coulombic efficiency in the cycling of anodes, and, for full cells, the coulombic efficiency can dictate the full cell's longevity. To confirm that this effect played a critical role in the performance of our cells, the two extreme cases, cell 1 and cell 4, were disassembled at the end-of-life (847 cycles for cell 1 and 223 cycles for cell 4), the anodes removed and gently rinsed with pure diethyl carbonate solvent, and SEM images taken to assess their morphology. As shown in Fig. 13, a rough surface was observed on the gently washed SNG12 particles of cell 4 that contained the PVDF binder, even though it cycled for far fewer cycles. Correspondingly, a smoother surface was observed for cell 1 with the PAALi binder. This smooth surface was uniformly coated with PAALi and was able to facilitate the efficient transportation of Li ions through the interface without excessive electrolyte reduction and, hence, good cycle life. The physical distribution of the binder appears to play an important role in the properties of the SEI layer and PAALi appears to do this more effectively than PVDF [20].

4. Conclusion

Electrodes containing SNG12 and $LiFePO_4$ fabricated with the aqueous-based binders PAA(H, Li, Na, and K) and an organic-based binder PVDF were evaluated for 1st cycle irreversible and reversible capacity, rate performance, and cycle life. The electrochemical results showed that PAA(H, Li, Na, and K) binders could significantly improve on all of these numbers except the rate capability for the SNG12 anodes as compared with electrodes fabricated from the traditional PVDF system. Among the PAAX series binders, PAALi and PAANa offered better cell performance, which is attributed to a more favorable polymer conformation in the composite. PAALi binder also improved the $LiFePO_4$ cathode's performance when compared to PVDF. As expected, the PAA(Li, Na, and K)-based binders resulted in brittle electrodes that showed macro-cracks upon drying; however, the cracks were suppressed if small amounts of SBR (0.5–3%) were added to the electrode in place of the PAAX. By employing different configurations of aqueous-based binders and conductive additives in SNG12 and $LiFePO_4$ electrodes, full cells could be cycled 847 times with 70% capacity retention, a 3-fold improvement over the traditional PVDF based system. This research suggests that water based PAAX series binders make for an attractive alternative to the traditional organic-solvent based PVDF system for natural graphite/$LiFePO_4$ cells, as the cycleability is improved, the manufacturing costs are lowered, and the potential negative impacts on the environment lessened.

Acknowledgement

This research was funded by the Assistant Secretary for Energy Efficiency, Office of Vehicle Technologies of the U.S. Department of Energy as part of the BATT program under contract no. DE-AC02-05CH11231.

References

[1] H. Maleki, G.P. Deng, I. Kerzhner-Haller, A. Anani, J.N. Howard, J. Electrochem. Soc. 147 (2000) 4470.
[2] K. Zaghib, K. Striebel, A. Guerfi, J. Shim, M. Armand, M. Gauthier, Electrochim. Acta 50 (2004) 263.
[3] G. Liu, H. Zheng, A.S. Simens, A.M. Minor, X. Song, V.S. Battaglia, J. Electrochem. Soc. 154 (2007) A1129.
[4] J. Li, L. Christensen, M.N. Obrovac, K.C. Hewitt, J.R. Dahn, J. Electrochem. Soc. 155 (2008) A234.
[5] D.W. Choi, D.H. Wang, V.V. Viswanathan, I.T. Bae, W. Wang, Z.M. Nie, J.G. Zhang, G.L. Graff, J. Liu, Z.G. Yang, T. Duong, Electrochem. Commun. 12 (2010) 378.
[6] A. Fedorkova, R. Orinakova, A. Orinak, I. Talian, A. Heile, H.D. Wiemhofer, D. Kaniansky, H.F. Arlinghaus, J. Power Sources 195 (2010) 3907.
[7] S.F. Lux, F. Schappacher, A. Balducci, S. Passerini, M. Winter, J. Electrochem. Soc. 157 (2010) A320.
[8] W. Porcher, B. Lestriez, S. Jouanneau, D. Guyomard, J. Electrochem. Soc. 156 (2009) A133.
[9] W. Porcher, P. Moreau, B. Lestriez, S. Jouanneau, D. Guyomard, Electrochem. Solid-State Lett. 11 (2008) A4.
[10] W. Porcher, P. Moreau, B. Lestriez, S. Jouanneau, F. Le Cras, D. Guyomard, Ionics 14 (2008) 583.
[11] A. Guerfi, M. Kaneko, M. Petitclerc, M. Mori, K. Zaghib, J. Power Sources 163 (2007) 1047.
[12] J.H. Lee, J.S. Kim, Y.C. Kim, D.S. Zang, U. Paik, Ultramicroscopy 108 (2008) 1256.
[13] W.R. Liu, M.H. Yang, H.C. Wu, S.M. Chiao, N.L. Wu, Electrochem. Solid-State Lett. 8 (2005) A100.

[14] N.S. Hochgatterer, M.R. Schweiger, S. Koller, P.R. Raimann, T. Wohrle, C. Wurm, M. Winter, Electrochem. Solid-State Lett. 11 (2008) A76.
[15] D. Mazouzi, B. Lestriez, L. Roue, D. Guyomard, Electrochem. Solid-State Lett. 12 (2009) A215.
[16] J.S. Bridel, T. Azais, M. Morcrette, J.M. Tarascon, D. Larcher, Chem. Mater. 22 (2010) 1229.
[17] J. Li, R.B. Lewis, J.R. Dahn, Electrochem. Solid-State Lett. 10 (2007) A17.
[18] H.Y. Wang, T. Umeno, K. Mizuma, M. Yoshio, J. Power Sources 175 (2008) 886.
[19] S. Komaba, K. Okushi, T. Ozeki, H. Yui, Y. Katayama, T. Miura, T. Saito, H. Groult, Electrochem. Solid-State Lett. 12 (2009) A107.
[20] J. Li, D.B. Le, P.P. Ferguson, J.R. Dahn, Electrochim. Acta 55 (2010) 2991.
[21] B. Lestrie, S. Bahri, I. Sandu, L. Roue, D. Guyomard, Electrochem. Commun. 9 (2007) 2801.
[22] C.W. Wang, A.M. Sastry, K.A. Striebel, K. Zaghib, J. Electrochem. Soc. 152 (2005) A1001.
[23] R.R. Garsuch, D.B. Le, A. Garsuch, J. Li, S. Wang, A. Farooq, J.R. Dahn, J. Electrochem. Soc. 155 (2008) A721.
[24] K.A. Hirasawa, K. Nishioka, T. Sato, S. Yamaguchi, S. Mori, J. Power Sources 69 (1997) 97.